The 1st Joint International Conference on Multibody System Dynamics
May 25–27, 2010, Lappeenranta, Finland

Flexible multibody modelling for the mechatronic design of compliant mechanisms

Ronald G.K.M. Aarts, Johannes van Dijk, Ben J.B. Jonker

Faculty of Engineering Technology, University of Twente
P.O. Box 217, 7500 AE Enschede, The Netherlands
e-mail: R.G.K.M.Aarts@utwente.nl, J.vanDijk@utwente.nl, J.B.Jonker@utwente.nl

ABSTRACT

In high precision equipment the use of compliant mechanisms is favourable as elastic joints offer the advantages of low friction and no backlash. To satisfy exact constraint design the mechanism should have exactly the required degrees of freedom and constraints so that the system is kinematically and statically determinate. For this purpose we propose the following kinematic analysis using a flexible multibody modelling approach. In compliant mechanisms the system's degrees of freedom are presented clearly from the analysis of a system in which the compliant part are free to deform while the support is considered rigid. If the Jacobian matrix associated with the dependent coordinates is not full column or row rank, the system is underconstraint or overconstraint. The rank of this matrix is calculated from a singular value decomposition. For an underconstraint system any motion in the mechanism that is not accounted for by the current set of degrees of freedom is visualised using data from the left singular matrix. For an overconstraint system a statically indeterminate stress distribution is derived from the right singular matrix and is used to visualise the overconstraints. In the next step of the mechatronic design the system's closed-loop stability and performance are considered. Valuable insight is obtained from a dynamic analysis in which the non-linear models are linearised in selected configurations to derive natural frequencies and mode shapes.

Keywords: exact constraint design, geometrically non-linear behaviour, kinematically indeterminate motion, statically indeterminate stress distribution, natural frequencies.

1 INTRODUCTION

In high precision equipment friction and backlash limit the achievable performance. Compliant mechanisms are favourable as the elastic joints in these systems allow motion with low friction and no backlash. In this paper we address the mechatronic design of these compliant mechanisms. In particular at the conceptual design stage there is no need for very detailed and complex models that are time-consuming to analyse. Nevertheless the models should capture the dominant system behaviour which must include relevant three-dimensional motion and geometric non-linearities, in particular when the system undergoes large deflections. We distinguish two phases in the modelling approach of which a kinematic design is the first phase. Typical design considerations for this phase aim e.g. at avoiding overconstraint design in line with so-called Exact Constraint Design principles [2, 8]. Recognising and repairing an underconstraint of overconstraint condition in a complicated system is not a trivial task. Once the kinematic design is accepted, the dynamic system performance is considered in the second design phase. In a mechatronic system natural frequencies and the accompanying mode shapes are closely related to the required closed-loop bandwidth [1].

In this paper we address the use of flexible multibody modelling with the SPACAR software package [9] for the design of such systems. This flexible multibody approach is based on non-linear finite elements and is well-suited to create the models for these analyses. Due to the definition of physical meaningful deformation modes and the sound inclusion of the non-linear geometrical effects at the element level [6] only a rather small number of elastic beam elements are needed to model typical elastic components accurately. The low-dimensional models prove to be well-suited for the kinematic analysis. For the dynamic analysis configuration dependent linearised models can be generated for control system design [5].

The modelling approach is briefly summarised in the next section. In section 3 is outlined how overconstraint and underconstraint systems can be analysed. This procedure is applied to the example of a straight guiding mechanism in section 4. The exact constraint design is verified with a kinematic analysis that is followed by a dynamic analysis to determine the relevant natural frequencies and accompanying mode shapes. Section 6 summarised the conclusions.

2 FINITE ELEMENT MODELLING

In this paper compliant mechanisms are modelled with a multibody system approach. The formulation is based on non-linear finite elements. The multibody system is modelled as an assembly of rigid body structures interconnected through a variety of connections such as flexible hinges and beams. The location of each element k is described relative to a fixed inertial coordinate system by a set of nodal coordinates $\boldsymbol{x}^{(k)}$, valid for large displacements and rotations. Translational and rotational coordinates are used to describe the Cartesian coordinates of the end nodes and the orientation of orthogonal base vectors or triads, rigidly attached to the element nodes.

Essential is the definition of the deformation modes of the element. The deformation modes are specified by a vector of deformation parameters $\boldsymbol{e}^{(k)}$ that are invariant for rigid body motions of the element [4]. The number of deformation parameters is equal to the number of nodal coordinates minus the number of degrees of freedom of the element as a rigid body. The deformation modes are explicitly described as non-linear deformation functions of the nodal coordinates

$$\boldsymbol{e}^{(k)} = \boldsymbol{\mathcal{D}}^{(k)}(\boldsymbol{x}^{(k)}). \tag{1}$$

In the example of a spatial beam element, there are twelve independent nodal coordinates and six rigid body degrees of freedom, so that six independent deformation modes can be defined. For the spatial flexible beam one deformation mode ε_1 is taken to describe the elongation, ε_2 for torsion and four modes ε_3–ε_6 for the bending deformations of the element [6, 7]:

$$\begin{aligned}
\varepsilon_1 &= \bar{\varepsilon}_1 + (2\bar{\varepsilon}_3^2 + \bar{\varepsilon}_3\bar{\varepsilon}_4 + 2\bar{\varepsilon}_4^2 + 2\bar{\varepsilon}_5^2 + \bar{\varepsilon}_5\bar{\varepsilon}_6 + 2\bar{\varepsilon}_6^2)/(30l_0) \\
&\quad + c_t\bar{\varepsilon}_2^2/(2l_0^3), \\
\varepsilon_2 &= \bar{\varepsilon}_2 + (-\bar{\varepsilon}_3\bar{\varepsilon}_6 + \bar{\varepsilon}_4\bar{\varepsilon}_5)/l_0, \\
\varepsilon_3 &= \bar{\varepsilon}_3 + \bar{\varepsilon}_2(\bar{\varepsilon}_5 + \bar{\varepsilon}_6)/(6l_0), \\
\varepsilon_4 &= \bar{\varepsilon}_4 - \bar{\varepsilon}_2(\bar{\varepsilon}_5 + \bar{\varepsilon}_6)/(6l_0), \\
\varepsilon_5 &= \bar{\varepsilon}_5 - \bar{\varepsilon}_2(\bar{\varepsilon}_3 + \bar{\varepsilon}_4)/(6l_0), \\
\varepsilon_6 &= \bar{\varepsilon}_6 + \bar{\varepsilon}_2(\bar{\varepsilon}_3 + \bar{\varepsilon}_4)/(6l_0),
\end{aligned}
\quad \text{with} \quad
\begin{aligned}
\bar{\varepsilon}_1 &= l - l_0, \\
\bar{\varepsilon}_2 &= l_0(\boldsymbol{e}_z^p \cdot \boldsymbol{e}_y^q - \boldsymbol{e}_y^p \cdot \boldsymbol{e}_z^q)/2, \\
\bar{\varepsilon}_3 &= -l_0\boldsymbol{e}_l \cdot \boldsymbol{e}_z^p, \\
\bar{\varepsilon}_4 &= l_0\boldsymbol{e}_l \cdot \boldsymbol{e}_z^q, \\
\bar{\varepsilon}_5 &= l_0\boldsymbol{e}_l \cdot \boldsymbol{e}_y^p, \\
\bar{\varepsilon}_6 &= -l_0\boldsymbol{e}_l \cdot \boldsymbol{e}_y^q,
\end{aligned} \tag{2}$$

where l is the distance between the nodal points, l_0 is the reference length of the element and $\boldsymbol{e}_l$ is the unit vector directed from node p to node q. The term with the torsional constant c_t accounts for torsion–elongation coupling [7]. Figure 1 illustrates five of these deformation modes and most of the unit vectors in the expressions. The elements account for geometric nonlinear effects such as geometric stiffening and interaction between deformation modes. Consequently, accurate models can be obtained with a small numbers of elements even for the case when large deformations are considered [6, 7].

For the entire multibody system the assembly of finite elements is realised by defining a global vector $\boldsymbol{x}$ of all nodal coordinates. The deformation functions of the elements constituting the multibody system can

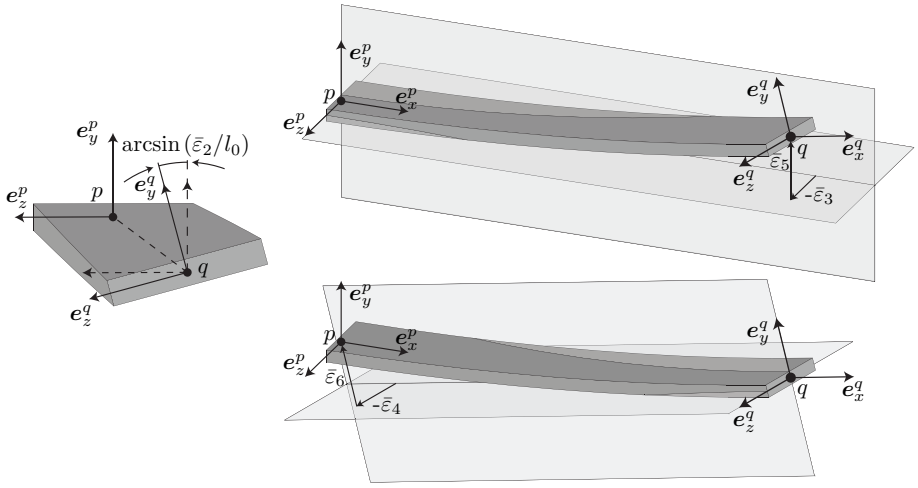

Figure 1. Deformations ε_2-ε_6 of the spatial beam element [7] (reprinted from [3]).

then be described in terms of the components of vector $\boldsymbol{e}$ yielding the non-linear vector function

$$\boldsymbol{e} = \boldsymbol{\mathcal{D}}(\boldsymbol{x}), \tag{3}$$

which represents the basic equations for the kinematic analysis. Kinematic constraints can be introduced by putting conditions on the nodal coordinates, denoted with $\boldsymbol{x}^{(o)}$ for support coordinates, as well as by prescribing the deformation parameters $\boldsymbol{e}^{(o)}$ to be zero for rigid bodies. In this paper all kinematic constraints are assumed to be holonomic.

An important notion in the kinematic and dynamic analysis of mechanical systems is that of degrees of freedom (DOF's). The number of kinematic degrees of freedom is the smallest number of coordinates n_{dof} that describe, together with the fixed, time-independent kinematic constraints, the configuration of the multibody system. We call them independent or generalised coordinates $\boldsymbol{q}$ which can be either absolute generalised coordinates, denoted $\boldsymbol{x}^{(m)}$, as well as relative generalised coordinates, denoted $\boldsymbol{e}^{(m)}$. In accordance with the above specified constraints and the choice of generalised coordinates, the vectors $\boldsymbol{x}$ and $\boldsymbol{e}$ can now be partitioned as

$$\boldsymbol{x} = \begin{bmatrix} \boldsymbol{x}^{(o)} \\ \boldsymbol{x}^{(c)} \\ \boldsymbol{x}^{(m)} \end{bmatrix} \quad \text{and} \quad \boldsymbol{e} = \begin{bmatrix} \boldsymbol{e}^{(o)} \\ \boldsymbol{e}^{(m)} \\ \boldsymbol{e}^{(c)} \end{bmatrix}, \tag{4}$$

where the superscript o denotes invariant nodal coordinates or deformations having a fixed prescribed value, the superscript c denotes dependent nodal coordinates or deformations and the superscript m denotes independent (or generalised) nodal coordinates or deformations. If the constraints are independent, the nodal coordinates and deformation parameters can be expressed as functions of the generalised coordinates $\boldsymbol{q} = (\boldsymbol{x}^{(m)}, \boldsymbol{e}^{(m)})$. With these expressions the system's equations of motion are derived according to [5] as a set of second order ordinary differential equations in terms of the kinematic degrees of freedom $\boldsymbol{q}$:

$$\bar{\boldsymbol{M}}(\boldsymbol{q})\ddot{\boldsymbol{q}} = \mathbf{D}_q \boldsymbol{\mathcal{F}}^{(x)T} \left(\boldsymbol{f} - \boldsymbol{M} \mathbf{D}_q^2 \boldsymbol{\mathcal{F}}^{(x,c)} \dot{\boldsymbol{q}} \dot{\boldsymbol{q}} \right) - \mathbf{D}_q \boldsymbol{\mathcal{F}}^{(e)T} \boldsymbol{\sigma}, \tag{5}$$

where $\bar{\boldsymbol{M}}$ is the system mass matrix computed from the global mass matrix M. The notations $\mathbf{D}_q \boldsymbol{\mathcal{F}}$ and $\mathbf{D}_q^2 \boldsymbol{\mathcal{F}}$ denote so-called first and second order geometric transfer functions [5]. The vector $\boldsymbol{f}$ are the nodal forces. Generalised stress resultants represent the loading state of each element and are assembled in the vector $\boldsymbol{\sigma}$. The unknown stress resultants and reaction forces are computed from the equations of reaction

$$(\mathbf{D}_x \boldsymbol{\mathcal{D}})^T \boldsymbol{\sigma} = \boldsymbol{f} - \boldsymbol{M}\ddot{\boldsymbol{x}}, \tag{6}$$

where differentiation operator $\mathbf{D}_x$ represents partial differentiation with respect to the nodal coordinates $\boldsymbol{x}$.

For further analyses or (linear) control system design, the non-linear equations of motion (5) and reaction (6) can be linearised. In [5] a linearised input-output representation of flexible multibody systems is presented as a set of state space equations in which an arbitrary combination of positions, velocities, accelerations, and forces can be taken as input variables and as output variables. From the (locally) linearised system equation the natural frequencies and accompanying mode shapes follow directly.

3 OVERCONSTRAINT AND UNDERCONSTRAINT SYSTEMS

The non-linear and linear analyses summarised above rely on a consistent selection of the constraints and independent or generalised coordinates. This aspect will be addressed in more detail next.

3.1 Kinematically indeterminate or underconstraint system

By differentiating Eq. (3) to time and using the chain rule, it appears that the velocities $\dot{\boldsymbol{x}}$ and $\dot{\boldsymbol{e}}$ must obey

$$\dot{\boldsymbol{e}} = (\mathbf{D}_x \boldsymbol{\mathcal{D}}) \dot{\boldsymbol{x}}. \tag{7}$$

With the partitioning of Eq. (4) for $\boldsymbol{x}$ and $\boldsymbol{e}$ this expression can be written as

$$\begin{bmatrix} \dot{\boldsymbol{e}}^{(o)} \\ \dot{\boldsymbol{e}}^{(m)} \\ \dot{\boldsymbol{e}}^{(c)} \end{bmatrix} = \begin{bmatrix} \mathbf{D}^{(o)}\boldsymbol{\mathcal{D}}^{(o)} & \mathbf{D}^{(c)}\boldsymbol{\mathcal{D}}^{(o)} & \mathbf{D}^{(m)}\boldsymbol{\mathcal{D}}^{(o)} \\ \mathbf{D}^{(o)}\boldsymbol{\mathcal{D}}^{(m)} & \mathbf{D}^{(c)}\boldsymbol{\mathcal{D}}^{(m)} & \mathbf{D}^{(m)}\boldsymbol{\mathcal{D}}^{(m)} \\ \mathbf{D}^{(o)}\boldsymbol{\mathcal{D}}^{(c)} & \mathbf{D}^{(c)}\boldsymbol{\mathcal{D}}^{(c)} & \mathbf{D}^{(m)}\boldsymbol{\mathcal{D}}^{(c)} \end{bmatrix} \begin{bmatrix} \dot{\boldsymbol{x}}^{(o)} \\ \dot{\boldsymbol{x}}^{(c)} \\ \dot{\boldsymbol{x}}^{(m)} \end{bmatrix}, \tag{8}$$

in which the derivative function $\mathbf{D}_x\boldsymbol{\mathcal{D}}$ is split in components where the parts of the deformation functions are differentiated with respect to a part of the nodal coordinates. The indicated submatrix

$$\boldsymbol{D}_{cc} = \begin{bmatrix} \mathbf{D}^{(c)}\boldsymbol{\mathcal{D}}^{(o)} \\ \mathbf{D}^{(c)}\boldsymbol{\mathcal{D}}^{(m)} \end{bmatrix} \tag{9}$$

is called the Jacobian matrix associated with the dependent coordinates $\boldsymbol{x}^{(c)}$. It relates the velocities of the dependent coordinates $\dot{\boldsymbol{x}}^{(c)}$ with the constraint deformations $\dot{\boldsymbol{e}}^{(o)}$ and velocities of the generalised coordinates $\dot{\boldsymbol{e}}^{(m)}$, $\dot{\boldsymbol{x}}^{(m)}$ as

$$\boldsymbol{D}_{cc}\,\dot{\boldsymbol{x}}^{(c)} = \begin{bmatrix} \dot{\boldsymbol{e}}^{(o)} \\ \dot{\boldsymbol{e}}^{(m)} \end{bmatrix} - \begin{bmatrix} \mathbf{D}^{(m)}\boldsymbol{\mathcal{D}}^{(o)} \\ \mathbf{D}^{(m)}\boldsymbol{\mathcal{D}}^{(m)} \end{bmatrix} \dot{\boldsymbol{x}}^{(m)}, \tag{10}$$

where the term with $\dot{\boldsymbol{x}}^{(o)} = 0$ has been omitted. If the inverse of matrix $\boldsymbol{D}_{cc}$ exists, the velocities $\dot{\boldsymbol{x}}^{(c)}$ can be computed from the constraints $\dot{\boldsymbol{e}}^{(o)} = 0$ and the velocities of the generalised coordinates $\dot{\boldsymbol{e}}^{(m)}$, $\dot{\boldsymbol{x}}^{(m)}$. For the existence of this inverse the matrix must be square. This implies that the dimension of $\boldsymbol{x}^{(c)}$ is equal to the sum of the dimensions of $\boldsymbol{e}^{(0)}$ and $\boldsymbol{e}^{(m)}$. The number of dependent coordinates $\boldsymbol{x}^{(c)}$ is the total number of coordinates minus the numbers of constraint coordinates $\boldsymbol{x}^{(o)}$ and independent generalised nodal coordinates $\boldsymbol{x}^{(m)}$. Then $\boldsymbol{D}_{cc}$ is square if the number of all kinematic degrees of freedom n_{dof} is equal to the number of nodal coordinates $\boldsymbol{x}$ minus the number of absolute and holonomic constraints, $\boldsymbol{x}^{(o)}$ and $\boldsymbol{e}^{(o)}$.

This is a necessary condition for the existence of $\boldsymbol{D}_{cc}^{-1}$ as it results in a square matrix $\boldsymbol{D}_{cc}$. It is not a sufficient condition as $\boldsymbol{D}_{cc}$ must also be non-singular, or equivalently the matrix $\boldsymbol{D}_{cc}$ should be full rank. For any square or rectangular matrix the rank can be determined from its singular value decomposition which for $\boldsymbol{D}_{cc}$ can be written as

$$\boldsymbol{D}_{cc} = \boldsymbol{U}\boldsymbol{\Sigma}\boldsymbol{V}^T, \tag{11}$$

in which $\boldsymbol{U}$ is an orthogonal $m \times m$ matrix, $\boldsymbol{V}$ is an orthogonal $n \times n$ matrix and matrix $\boldsymbol{\Sigma}$ is an $m \times n$ diagonal matrix with non-negative real numbers on the diagonal, denoting m the number of rows in $\boldsymbol{D}_{cc}$ and n the number of columns. The inverse of $\boldsymbol{D}_{cc}$ exists if the matrix is square, i.e. $m = n$, and all singular values are non-zero.

If some of the singular values are zero, or more generally, if $\boldsymbol{D}_{cc}$ is not full column rank, it can be seen from Eq. (10) that there is a non-zero solution for $\dot{\boldsymbol{x}}^{(c)}$ that satisfies the constraint $\dot{\boldsymbol{e}}^{(o)} = 0$ while the velocities of the generalised coordinates $\dot{\boldsymbol{e}}^{(m)}$, $\dot{\boldsymbol{x}}^{(m)}$ are also zero. That means the system is *kinematically indeterminate* or *underconstraint*. Matrix $\boldsymbol{D}_{cc}$ is column rank deficient if there are more columns than rows, i.e. $n > m$. In addition zero singular values increase the column rank deficiency. By combining the singular value decomposition (11) with Eq. (8) it can be seen that each column in $\boldsymbol{V}$ accompanying one of the zero singular values or excess columns specifies a vector of velocities $\dot{\boldsymbol{x}}^{(c)}$ which represents the motion of a kinematically indeterminate mode.

3.2 Statically indeterminate or overconstraint system

For the solution of the equations of motion (5) and reaction (6), the nodal force vector $\boldsymbol{f}$ and the vector of generalised stress resultants $\boldsymbol{\sigma}$ are also partitioned in accordance with Eq. (4) as

$$\boldsymbol{f} = \begin{bmatrix} \boldsymbol{f}^{(o)} \\ \boldsymbol{f}^{(c)} \\ \boldsymbol{f}^{(m)} \end{bmatrix} \quad \text{and} \quad \boldsymbol{\sigma} = \begin{bmatrix} \boldsymbol{\sigma}^{(o)} \\ \boldsymbol{\sigma}^{(m)} \\ \boldsymbol{\sigma}^{(c)} \end{bmatrix}. \tag{12}$$

With this partitioning and considering a stationary configuration in which accelerations are zero, Eq. (6) is written as:

$$\begin{bmatrix} (\mathbf{D}^{(o)}\boldsymbol{\mathcal{D}}^{(o)})^T & (\mathbf{D}^{(o)}\boldsymbol{\mathcal{D}}^{(m)})^T & (\mathbf{D}^{(o)}\boldsymbol{\mathcal{D}}^{(c)})^T \\ (\mathbf{D}^{(c)}\boldsymbol{\mathcal{D}}^{(o)})^T & (\mathbf{D}^{(c)}\boldsymbol{\mathcal{D}}^{(m)})^T & (\mathbf{D}^{(c)}\boldsymbol{\mathcal{D}}^{(c)})^T \\ (\mathbf{D}^{(m)}\boldsymbol{\mathcal{D}}^{(o)})^T & (\mathbf{D}^{(m)}\boldsymbol{\mathcal{D}}^{(m)})^T & (\mathbf{D}^{(m)}\boldsymbol{\mathcal{D}}^{(c)})^T \end{bmatrix} \begin{bmatrix} \boldsymbol{\sigma}^{(o)} \\ \boldsymbol{\sigma}^{(m)} \\ \boldsymbol{\sigma}^{(c)} \end{bmatrix} = \begin{bmatrix} \boldsymbol{f}^{(o)} \\ \boldsymbol{f}^{(c)} \\ \boldsymbol{f}^{(m)} \end{bmatrix}. \tag{13}$$

The matrix in the lefthand side is the transpose of the derivative function $\mathbf{D}_x\boldsymbol{\mathcal{D}}$ in Eq. (8). Hence, the transpose of submatrix $\boldsymbol{D}_{cc}$ can also be recognised which gives an expression for the generalised stress

resultants $\boldsymbol{\sigma}^{(o)}$ and $\boldsymbol{\sigma}^{(m)}$ as

$$\boldsymbol{D}_{cc}^T \begin{bmatrix} \boldsymbol{\sigma}^{(o)} \\ \boldsymbol{\sigma}^{(m)} \end{bmatrix} = \boldsymbol{f}^{(c)} - (\mathbf{D}^{(c)}\boldsymbol{\mathcal{D}}^{(c)})^T \boldsymbol{\sigma}^{(c)}. \tag{14}$$

If the inverse of $\boldsymbol{D}_{cc}$ exists, then also the inverse of its transpose $\boldsymbol{D}_{cc}^T$ exists and the generalised stress resultants $\boldsymbol{\sigma}^{(o)}$ and $\boldsymbol{\sigma}^{(m)}$ that are dual to the relative constraints $\boldsymbol{e}^{(o)}$ and independent deformation mode coordinates $\boldsymbol{e}^{(m)}$ can be computed from the nodal forces and the other generalised stress resultants in the righthand side of Eq. (14). In the case $\boldsymbol{D}_{cc}^T$ is not full column rank a non-zero solution of the generalised stress resultants $\boldsymbol{\sigma}^{(o)}$ and $\boldsymbol{\sigma}^{(m)}$ exists for which the nodal forces $\boldsymbol{f}^{(c)}$ and generalised stress resultants $\boldsymbol{\sigma}^{(c)}$ are zero. This indicates a *statically indeterminate* or *overconstraint* system.

Note that the column rank of $\boldsymbol{D}_{cc}^T$ equals the row rank of $\boldsymbol{D}_{cc}$. Matrix $\boldsymbol{D}_{cc}$ is row deficient if there are more rows than columns, i.e. $m > n$, or there are zero singular values. From Eq. (11) the singular value decomposition of $\boldsymbol{D}_{cc}^T$ follows immediately as

$$\boldsymbol{D}_{cc}^T = \boldsymbol{V}\boldsymbol{\Sigma}^T\boldsymbol{U}^T. \tag{15}$$

By combining this singular value decomposition with Eq. (13), we recognise that each column in $\boldsymbol{U}$ accompanying one of the zero singular values or an excess row of $\boldsymbol{D}_{cc}$ gives a non-zero solution of the generalised stress resultants $\boldsymbol{\sigma}^{(o)}$ and $\boldsymbol{\sigma}^{(m)}$ that represent a set of statically indeterminate stresses.

3.3 Kinematic analysis and visualisation

In Table 1 it is summarised that row and/or column rank deficiency of matrix $\boldsymbol{D}_{cc}$ implies a statically and/or kinematically indeterminate system. Moreover with each excess row or column and with each zero singular value there is a column in the matrix $\boldsymbol{U}$ or $\boldsymbol{V}$ that describes the indeterminate mode. The kinematically indeterminate modes are found in matrix $\boldsymbol{V}$ and can directly be used to visualise a motion of the system, i.e. a non-zero velocity $\dot{\boldsymbol{x}}^{(c)}$. The statically indeterminate modes are found in matrix $\boldsymbol{U}$ and give non-zero generalised stress resultants $\boldsymbol{\sigma}^{(o)}$, $\boldsymbol{\sigma}^{(m)}$. These can be visualised as a statically indeterminate stress distribution in the elements using the analysis presented by Boer *et al.* [3].

To illustrate this approach we consider the system with twelve rigid trusses shown in Figure 2. Eight trusses are supported in four supports the $z=0$ plane with coordinates $(\pm 1, \pm 1, 0)$. They are interconnected in the $z=1$ plane in the points $(1,0,1)$, $(0,1,1)$, $(-1,0,1)$, $(0,-1,1)$. Four trusses connect these points also directly as shown in the figure. In the eight support and connection points the trusses can rotate freely. In SPACAR each truss element connects two Cartesian nodal points and has only one deformation which is its elongation ε_1. Only Cartesian coordinates are needed to analyse this system. There are $4 \times 3 = 12$ support coordinates $\boldsymbol{x}^{(o)}$ (in the $z=0$ plane). The nodes in the $z=1$ give $4 \times 3 = 12$ dependent coordinates $\boldsymbol{x}^{(c)}$. There are 12 constraint deformations $\boldsymbol{e}^{(o)}$ counting the elongations in all trusses. Hence $\boldsymbol{D}_{cc}$ is a square 12×12 matrix. Counting the number of degrees of freedom results in $n_{\mathrm{dof}} = 0$, suggesting that the system is a structures and should not move.

However, the smallest singular value of this system appears to be zero indicating that the system has both one statically indeterminate mode and one kinematically indeterminate mode. The motion associated with

$m = n$	$\mathrm{rank}(\boldsymbol{D}_{cc}) = m = n$	statically determinate	kinematically determinate
	$\mathrm{rank}(\boldsymbol{D}_{cc}) < m = n$	statically indeterminate	kinematically indeterminate
$m > n$	$\mathrm{rank}(\boldsymbol{D}_{cc}) = n < m$	statically indeterminate	kinematically determinate
	$\mathrm{rank}(\boldsymbol{D}_{cc}) < n < m$	statically indeterminate	kinematically indeterminate
$m < n$	$\mathrm{rank}(\boldsymbol{D}_{cc}) = m < n$	statically determinate	kinematically indeterminate
	$\mathrm{rank}(\boldsymbol{D}_{cc}) < m < n$	statically indeterminate	kinematically indeterminate

Table 1. System properties depending on the number of rows m, the number of columns n and the rank of matrix $\boldsymbol{D}_{cc}$.

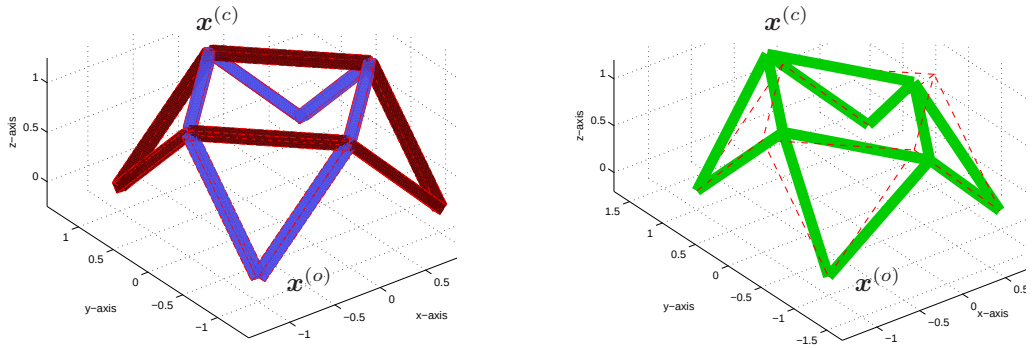

(a) statically indeterminate stress distribution (colours indicate sign of the stresses)

(b) kinematically indeterminate motion (dashes show the initial configuration)

Figure 2. System with 12 rigid trusses, supported in the $z = 0$ plane and connected in the $z = 1$ plane.

the latter follows from the last column of the right singular matrix $\boldsymbol{V}$:

Coordinates $\boldsymbol{x}^{(c)}$	Motion $\dot{\boldsymbol{x}}^{(c)}$ from $\boldsymbol{V}$
$(\ 0, -1,\ \ 1\ )$	$(\ 0\ , -0.5,\ \ 0\ )$
$(\ 1,\ \ 0,\ \ 1\ )$	$(-0.5,\ \ 0\ ,\ \ 0\ )$
$(\ 0,\ \ 1,\ \ 1\ )$	$(\ 0\ ,\ \ 0.5,\ \ 0\ )$
$(-1,\ \ 0,\ \ 1\ )$	$(\ 0.5,\ \ 0\ ,\ \ 0\ )$

(16)

Apparently, the square of the four trusses in the $z = 1$ can deform as is visualised in Figure 2(b). Note that the motion of the system is illustrated by assuming the velocity $\dot{\boldsymbol{x}}^{(c)}$ is applied for some finite time. The constraint equations for e.g. the elongations are then not necessarily satisfied. This would require a non-linear simulation of the motion which is not needed to illustrate the motion of the unconstraint mode.

The last column of the left singular matrix $\boldsymbol{U}$ represent the statically indeterminate stress resultants, which are the longitudinal stresses in the trusses. All values are non-zero and equal to $\pm\frac{1}{6}\sqrt{3}$, where half of the stress resultants show a negative sign and the other half are positive. The graph in Figure 2(a) shows these stress resultants where the different colours indicate the positive and negative stress resultants. The overconstraint condition can be avoided by allowing the elongation in one of the trusses. Note that the exact value of the stress resultants does not have a physical meaning as the vector with the stress resultants can be multiplied with any positive of negative constant to obtain another set of stress resultants representing an statically indeterminate mode.

4 EXACT CONSTRAINT DESIGN OF A COMPLIANT MECHANISM

Next it will be shown how the proposed analysis can be applied for the *exact constraint design* of a compliant mechanism. A system satisfies exact constraint design if it is both kinematically and statically determinate. According to Table 1 this implies that $\boldsymbol{D}_{cc}$ is square ($m = n$) and non-singular. As an example a straight guidance mechanism is considered in which some rigid part should move in one translational directions while all other motions must be suppressed.

4.1 Straight guidance mechanism

A typical approach for the design of the straight guidance mechanism is to assemble it from parts that confine one or more degrees of freedom each. To achieve an exact constraint design, no degree of freedom should be confined more than once and the desired translational motion of the system should not be constrained. In the concept of Figure 3(a) five wire flexures are applied. The longitudinal stiffness of the wire flexure is relatively high, while the stiffnesses for bending and torsion are rather small. So each wire flexure restricts only one degree of freedom being the translation along its longitudinal axis. The straight guidance can be achieved with any combination of five wire flexures that are not aligned with the direction of the intended motion and that do not confine the same degree of freedom more than once.

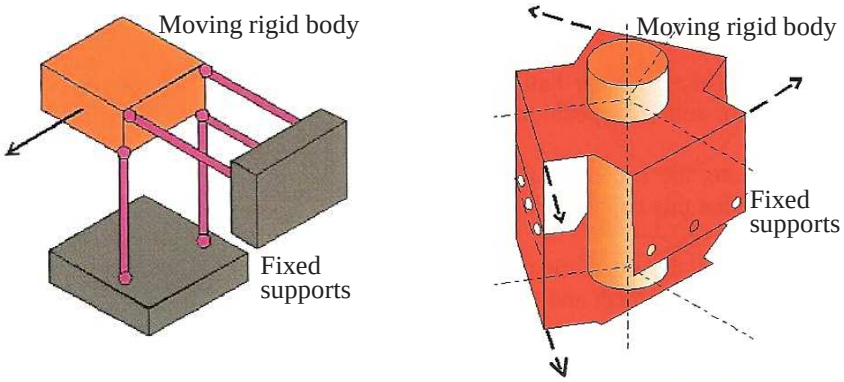

(a) five wire flexures (b) five folded sheet flexures

Figure 3. Two concepts for a one degree-of-freedom (1-DOF) straight guiding mechanism (reprinted from [8]). In (a) the solid arrow indicates the free movement. In (b) the cylinder represents the moving part. The supports are at the holes. The dashed arrows indicate directions of constraint movements.

A folded sheet flexure also restricts one degree of freedom as will be detailed in the next subsection. So five folded sheet flexures can also be used for the straight guidance as shown in Figure 3(b).

4.2 Kinematic analysis of wire flexures and folded sheet flexures

For the kinematic analysis of a system, the compliant parts are modelled such that the elastic deformations with low stiffness can deform, whereas the other deformations are suppressed. In the system with five wire flexures, Figure 3(a), each of the wire flexure supports is modelled with one beam element. One end of the beam is fully supported which means that all translational and rotational coordinates are fixed ($\boldsymbol{x}^{(o)}$). The wire flexure allows bending in either direction as well as torsion around its longitudinal axis. The relatively large longitudinal stiffness disallows elongation ε_1 of the element. So there is one zero deformation ($e^{(o)}$) in the element and the other five deformations are defined to be dependent ($\boldsymbol{e}^{(c)}$). For the coordinates at the free end of the wire flexure one constraint equation must be satisfied leaving five independent coordinates.

In the system of Figure 3(a) there are five wire flexures that are combined to define the motion of one rigid part. As each wire flexure adds one constraint for the translational and rotational coordinates of the motion of its free end, the combination of all five wire flexures leaves one degree of freedom if the constraints are independent. Matrix $\boldsymbol{D}_{cc}$ must be square as can be verified easily. The number of rows equals the number of constraint and independent deformations. In each wire flexure the elongation is fixed, so there are five rows. The number of columns equals the number of dependent coordinates. These coordinates are translational and rotational coordinates of the rigid body. If the intended translation is defined as the independent coordinate $x^{(m)}$, then five dependent coordinates remain and $\boldsymbol{D}_{cc}$ is indeed square.

Modelling the system with the folded sheet flexures, Figure 3(b), is somewhat more complicated. A support with a folded sheet flexure as shown in Figure 4(a) consists of two sheet flexures in series. Out of plane bending and torsion are allowed for each sheet flexure while the stiffnesses for bending in the plane of the sheet and elongation are high. For the kinematic analysis a beam element is used for each sheet in the flexure. Taking the local z axis of the beam element in the plane of the sheet as illustrated in Figure 1, the zero deformations are the elongation ε_1 and the bending deformations ε_3,ε_4 in the in-plane z direction. The torsion ε_2 and bending deformations ε_5,ε_6 in the out-of-plane y direction are other three deformation that can vary. Combining two sheets, there are six deformations in the folded sheet flexure that are not suppressed. It is not correct to define all these deformations to be dependent deformations as that would suggest that there are no constraints for the six coordinates of the free end. As shown in Figure 4(a) the folded sheet flexure imposes one constraint being a translation of the connection between the sheets. There is also an internal vibration mode, which is a rotation around the axis of this connection. Figure 4(b) illustrates that this internal mode can occur even if both ends of the folded sheet flexure are fixed.

The constraint and internal modes of the folded sheet flexure can be accounted for by taking one of the

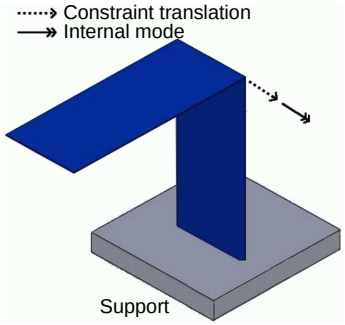

(a) single folded sheet flexure support

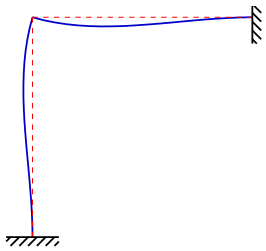

(b) internal vibration mode (side view)

Figure 4. Constraint translation and internal mode of a single folded sheet flexure.

bending deformations as an independent deformation, thus leaving five dependent deformations. In this way for the coordinates at the free end of the folded sheet flexure one constraint equation has to be satisfied leaving five independent coordinates similar as for the wire flexure. In addition, each folded sheet flexure exhibits one internal independent deformation.

Combining five folded sheet flexures as in the system of Figure 3(b) leave one independent coordinate for the cylindrical rigid body to which all flexures are attached, if the five constraints are independent. Also in this case matrix $\boldsymbol{D}_{cc}$ must be square. In each folded sheet flexure there are six constraint deformations and one independent deformation, so there are 35 rows in total. Counting the dependent coordinates, we observe that in each flexure the six coordinates of translation and rotation of the connection between the sheets are dependent. Furthermore, the rigid connection of all flexures has one independent coordinate, leaving five dependent coordinates. So $\boldsymbol{D}_{cc}$ has 35 columns and is indeed square. With SPACAR it can be verified that $\boldsymbol{D}_{cc}$ is non-singular for the configuration shown in Figure 3(b). The actual size of matrix $\boldsymbol{D}_{cc}$ is larger as there are more nodal points used to model the translating rigid part. As this part is rigid there is also a constraint deformation for every extra nodal coordinate, so $\boldsymbol{D}_{cc}$ remains square.

A drawback of this design is its asymmetry. A symmetric design can offer advantages e.g. to reduce position errors of the moving rigid part due to temperature changes. Also in the dynamic analyses to be discussed in the next section it appears that two folded flexures on one side offer a lower support stiffness compared to three folded flexures on the other side. More symmetric designs are presented in Figure 5. With five folded sheet flexures the symmetry at the lower end is improved by changing the position and orientation of one of the folded sheet flexures as shown in figure Figure 5(a). However, this does not increase the support stiffness and, even worse, a kinematic analysis reveals immediately that this design is both underconstraint

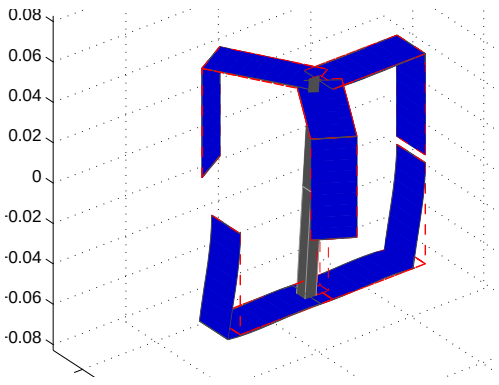

(a) Kinematically indeterminate motion

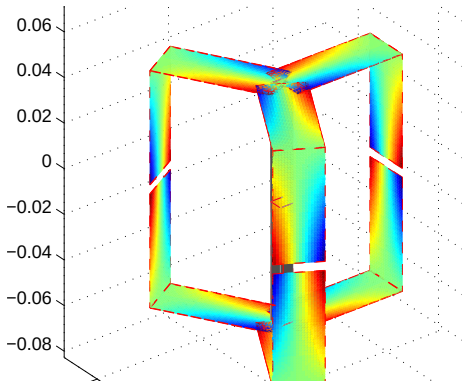

(b) Statically indeterminate stress distribution

Figure 5. Alternative straight guiding mechanisms: (a) overconstraint and underconstraint design with five folded sheet flexures, (b) overconstraint design with six folded sheet flexures.

and overconstraint. As the constraint degrees of freedom of both lower flexures are parallel, these constraints are not independent thus allowing the kinematically indeterminate motion shown in the figure.

With six folded sheet flexures the symmetric design of Figure 5(b) is realised. As the extra flexure adds an extra constraint, this design is overconstraint. The statically indeterminate stress distribution shown in the figure indicates an in-plane bending stress in all sheet flexures. If an exact constraint design must be realised, this can be accomplished by allowing this bending motion in one of the sheets or its support. Alternatively, a purely torsional deformation in the rigid body can be released.

5 Dynamic analysis with natural frequencies and mode shapes

For the dynamic analysis in the second phase more detailed models are used. Additional degrees-of-freedom are defined to study the non-ideal motion of the system reflecting e.g. the finite stiffness of the deformations so far considered to be rigid in the kinematic analysis. Including the mass and stiffness properties the natural frequencies and accompanying mode shapes can be obtained from linearised models. In a sound mechatronic design the lowest natural frequency should be associated with the intended motion of the system, while the higher natural frequencies play a crucial role for the closed-loop stability [1]. For a more accurate analysis of these high-frequent modes the elastic components like wire and sheet flexures may be divided into more than one elastic beam element although it was found that usually with only a small number of elements accurate and adequate models are obtained.

Figure 6(ab) shows the first and second vibration mode of the straight guiding mechanism with five folded sheet flexures as in Figure 3(b). In this analysis one beam is used to model each sheet. Masses and stiffnesses are calculated for steel sheets with dimensions: Length 50 mm, width 20 mm and thickness 0.2 mm. The total mass of the rigid part is 0.312 kg. With these numerical values a first natural frequency of 8.2 Hz is found. The next natural frequency is about 20 times larger. The accompanying mode shape is a rather asymmetric vibration, Figure 6(b). The asymmetry can be understood as the rigid part is supported by three and two flexures on either side. At the third natural frequency (282 Hz) the rigid body is also moving, while the fourth and next natural frequencies arise from the internal modes of the folded sheet flexures. For an accurate calculation of these internal vibration modes it is advisable to use two beam elements in each sheet. To determine the first three modes one beam element per sheet suffices.

Studying the vibration modes in somewhat more detail reveals that the second and third mode involve in-plane bending of sheet flexures. The second natural frequency is rather low as due to the asymmetric design a vibration mode is possible where only two sheet flexures need to undergo this in-plane bending. This observation stimulates the research into the design alternative with an extra folded sheet flexure as presented in Figure 5(b) in the previous section.

For a dynamic analysis of the overconstraint straight guiding mechanism with six folded sheet flexures a square matrix $\boldsymbol{D}_{cc}$ is obtained by defining one of the in-plane deformations to be dependent. The remaining in-plane deformations and the elongations are added to the generalised coordinates. It appears that the first

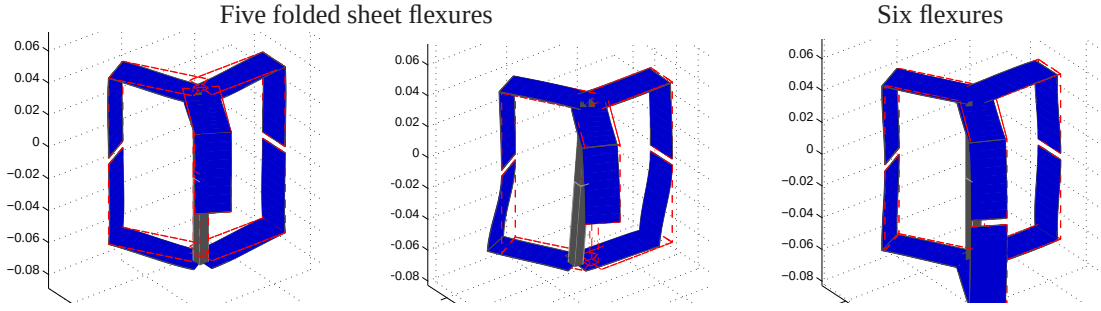

(a) First mode (8.2 Hz) (b) Second mode (163 Hz) (c) Second mode (282 Hz)

Figure 6. First and second mode shapes of the straight guiding mechanisms with five folded sheet flexures and the overconstraint design with six folded sheet flexures.

mode shape doesn't change although the first natural frequency increases to 9.0 Hz as the stiffness increases due to the extra flexure. The second mode shape is shown in Figure 6(c). The second natural frequency increases much more and coincides now with the third natural frequency. Apparently, in the symmetric design with an extra flexure the lowest support stiffness has been increased. The fourth and next natural frequencies represent again the internal modes of the flexures. To conclude, the kinematic and dynamic analysis clearly reveal advantages and disadvantages of the symmetric design with six folded sheet flexures. The extra flexures raises the second natural frequency, but also makes the system overconstraint. While the first result is beneficial for closed-loop stability, the second aspect may cause undesired behaviour e.g. if there are manufacturing inaccuracies.

6 CONCLUSIONS

The analysis of the simple 1-DOF straight guiding mechanisms illustrates how the flexible multibody approach of SPACAR is used for the conceptual mechatronic design. In the kinematic analysis all deformations with a high stiffness are defined to be invariant. Both kinematically and statically indeterminate modes can be visualised using data from the left and right singular matrices of the matric $\boldsymbol{D}_{cc}$. In this way a system satisfying exact constraint design can be obtained. In the subsequent dynamic analysis the finite support stiffness is accounted for. Natural frequencies and mode shapes are determined from a linearised model and provide essential insight for the expected closed-loop performance of the system. The low-dimensional models capture the dominant system behaviour which includes relevant three-dimensional motion and geometric non-linearities, in particular when the system undergoes large deflections.

ACKNOWLEDGEMENTS

The authors acknowledge the contributions from Jaap Meijaard to the singular value decomposition. Steven Boer and Tjeerd van der Poel contributed significantly to the postprocessing and visualisation.

REFERENCES

[1] AARTS, R. G., VAN DIJK, J., AND JONKER., B. J. Efficient analyses for the mechatronic design of mechanismswith flexible joints undergoing large deformations. In *ECCOMAS Thematic Conference Multibody Dynamics 2009* (Warsaw University of Technology, June 29 – July 2, 2009).

[2] BLANDING, D. *Exact Constraint: Machine Design Using Kinematic Principles*. ASME Press, New York, 1999.

[3] BOER, S. E., AARTS, R. G., BROUWER, D. M., AND JONKER, B. Multibody modelling and optimization of a curved hinge flexure. In *The 1st Joint International Conference on Multibody System Dynamics* (Lappeenranta, Finland, May 25-–27, 2010).

[4] JONKER, J. A finite element dynamic analysis of flexible spatial mechanisms and manipulators. *Comput. Methods Appl. Mech. Eng. 76* (1989), 17–40.

[5] JONKER, J., AARTS, R., AND VAN DIJK, J. A linearized input–output representation of flexible multibody systems for control synthesis. *Multibody System Dynamics 21,* 2 (2009), 99–122.

[6] JONKER, J., AND MEIJAARD, J. Definition of deformation parameters for the beam element and their use in flexible multibody system analysis. In *ECCOMAS Thematic Conference Multibody Dynamics 2009* (Warsaw University of Technology, June 29 – July 2, 2009).

[7] MEIJAARD, J., BROUWER, D., AND JONKER, J. Analytical and experimental investigation of a parallel leaf spring guidance. *Multibody System Dynamics 23,* 1 (2010), 77–97.

[8] SOEMERS, H. *Design Principles for Precision Mechanisms (lecture notes 113136)*. University of Twente, Enschede, The Netherlands, 2009.

[9] The SPACAR software package. http://www.spacar.nl/, 2010.